Case Studies in Thermal Engineering 39 (2022) 102476

Contents lists available at ScienceDirect

Case Studies in Thermal Engineering

journal homepage: www.elsevier.com/locate/csite

Analysis and optimization of flow and heat transfer performance of active thermal protection channel for hypersonic aircraft

Yancong Qiao [a], Peng Liu [c,**], Wei Liu [b], Zhichun Liu [a,b,*]

[a] China–EU Institute for Clean and Renewable Energy, Huazhong University of Science and Technology, Wuhan, 430074, China
[b] School of Energy and Power Engineering, Huazhong University of Science and Technology, Wuhan, 430074, China
[c] Institute of Thermal Science and Power Engineering, Wuhan Institute of Technology, Wuhan, 430205, China

ARTICLE INFO

Keywords:
Hypersonic aircraft
Active thermal protection
Diamond channel
RP–3
Symmetric longitudinal swirls

ABSTRACT

This paper presents a numerical simulation on the thermal–hydraulic performance of multiple parallel cooling channels to realize active thermal protection of hypersonic aircraft. The fluid velocity is set in the range of 0.5–2.5 m/s, with the corresponding Reynolds number of 4300 to 22,000, and results show that the rectangular and triangular channel have the best cooling performance on outer wall and inner wall with water as coolant, respectively. Further, "Diamond" channel is proposed to improve the cooling performance, and aviation kerosene RP–3 is used as coolant. Three inlet temperatures (243, 253 and 263 K) are applied to investigate the thermal protection performance of Diamond channel. The cooling performance of RP–3 is better than water, and total pump power of RP–3 is only 60% of water. It is found that the conspicuous symmetric longitudinal swirls generated at the leading edge effectively enhance the heat convection performance. Under the studied ranges of fluid velocity and inlet temperatures, outer and inner wall temperatures can be controlled below 700 K and 330 K, respectively. Subsequently, the preliminary parameters of the "Diamond" are investigated and optimized. Model with L = 16 mm, Yc = 3 and X = 8.8 mm has better thermal protection performance and mechanical properties.

1. Introduction

Hypersonic aircraft has become the representative of advanced flight technology which can cruise around the world definitely within extremely short time, thus its leading status in the future aviation field is established [1]. With the development of aerospace technology, the problem of aerodynamic heating faced by hypersonic aircraft is rising, and active cooling thermal protection system (ACTPS) plays an increasingly important role in hypersonic aircraft [2,3]. When hypersonic aircraft flies at high mach number, the surface is heated by strongly aerodynamic heating [4,5], which will lead to large heat flux density and excessive high local wall temperature [6–8]. Therefore, ACTPS is essential to the safe operation of hypersonic aircraft [9].

At present, there are many cooling mechanisms for hypersonic aircrafts. Scholars generally believe that it is feasible to cool the engine by regenerative cooling [10–14], but it is seldom used in small aero–engines because of weight problem [15,16]. Film cooling is also an efficient active cooling scheme in which a thin thermal insulation layer generated on the surface blocks the heat outside though its thermal protection for high heat flux is still limited [17]. In recent years, transpiration cooling has gradually developed [18–20]. Usually, the transpiration cooling of liquid rocket is mainly composed of two types of porous materials: porous laminate and sintered

* Corresponding author. China–EU Institute for Clean and Renewable Energy, Huazhong University of Science and Technology, Wuhan, 430074, China.
** Corresponding author.
E-mail addresses: peng_liu@wit.edu.cn (P. Liu), zcliu@hust.edu.cn (Z. Liu).

https://doi.org/10.1016/j.csite.2022.102476
Received 10 June 2022; Received in revised form 23 September 2022; Accepted 4 October 2022
Available online 5 October 2022

porous medium [21–25]. Otsu et al. [26] proved in 2007 that in the process of transpiration cooling, a small amount of coolant can dissipate a quantity of heat via transient vaporization. Su et al. [27] investigated the flow and heat transfer characteristics of leading edge, found that a large amount of coolant flowing to the tail which bears less thermal load, resulting in the coolant waste. In comparison, ACTPS is a feasible thermal protection scheme that can meet the flight conditions of hypersonic aircraft, and hydrocarbon fuel can be used as coolant [28–32]. Fang et al. [33] studied the pyrolysis of mixed endothermic hydrocarbon fuel and characterized a series of high temperature characteristics of hydrocarbon fuel. It is crucial to study the mechanical properties and thermal protection performance of ACTPS under the supersonic flight condition [34].

Numerous studies support that ACTPS has the advantages of long–time heating with high heat flux, closed–loop temperature control and reusability which make it a good choice for hypersonic aircraft thermal protection [35–38]. In NASA's third generation rocket based combined cycle power aircraft project, researchers proposed a sandwich structure made of alloy and carbon composite material, which successfully passed the test of scramjet [39]. Subsequently, relevant scholars have made a lot of research work on the material selection of hypersonic aircraft, and gradually established the development direction of the transition from metal tube matching composite structure to full composite structure. Hou et al. [40] proposed a thermal protection scheme of double honeycomb sandwich convective cooling. The results show that the structure has excellent heat dissipation performance. HA Jie et al. [41] studied the mechanism of combinational active thermal protection system (CA-TPS) of the hypersonic aircrafts by numerical method, which has significantly weaker reattachment shock wave than traditional spiked blunt body and reduces aeroheating directly. Liu et al. [42] designed a transpiration active cooling metal thermal protection system that can reduce the structure temperature about 50 K. Chen et al. [43] designed a cooling channel for an engine to realize the active thermal protection which verified that external vibrations would enhance the heat transfer characteristics of the cooling channel. Peng et al. [44] proposed the ceramic based active cooling structure which can meet the thermal protection requirement under high heat flux through less coolant flow.

The research of aircraft thermal protection is a complex project. In the 21st century, the layout of thermal protection system is developing towards the integration of "heat protection, structure and function" and "low cost, unification and high efficiency". This paper proposes an improved active thermal protection structure of hypersonic aircraft, investigates and compares the thermal protection performance of different flow channels. Besides, different coolants and various parameters are analyzed systematically by numerical simulation.

2. Model description

2.1. Physical model

In this work, we present in Fig. 1 (a) several parallel cooling channels with different flow–through section shapes whose coolant flows through each channel in parallel and quickly removes the aerodynamic heat from outer wall. For purpose of saving

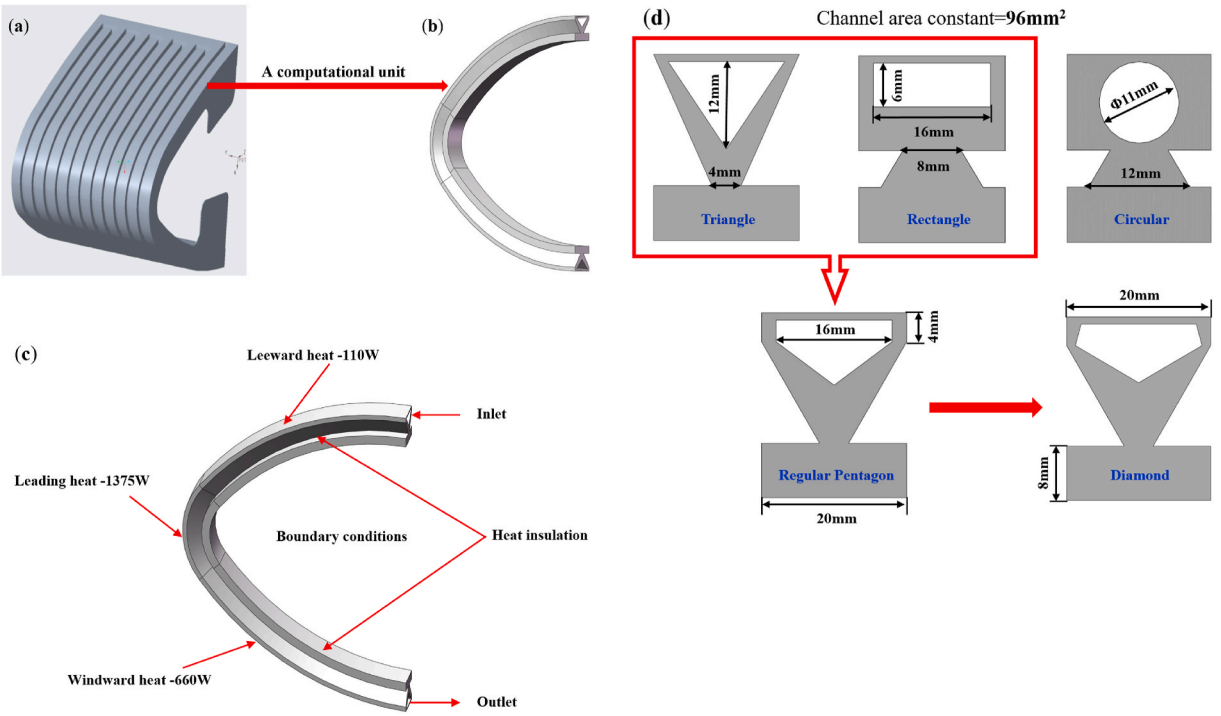

Fig. 1. Constructional schematic diagram of thermal protection object (a) overall appearance (b) channel unit (c) boundary conditions (d) geometric parameters of five channels.

computational resources, a channel unit is taken as the research object of theoretical analysis and numerical simulation, as depicted in Fig. 1 (b). Fig. 1 (c) shows the boundary conditions of the thermal protection structure which is composed of outer wall, inner wall, support structure and fluid domain. The aerodynamic heating power on leading edge, windward, and leeward surface are 1375 W, 660 W and 110 W respectively. Channel unit with different flow–through section shapes with a consistent area of 96 mm^2 are established, as shown in Fig. 1 (d). It should be pointed out that when flow area is too large, the remaining solid area will face the risk of not meeting the structural strength, while the larger coolant flow will greatly enhance the active thermal protection performance. After considering all the different flow–through section shapes, 96 mm^2 is chosen as the flow area. Likewise, the constructional parameters are given in Fig. 1 (d). The total width is 20 mm, the thickness of outer wall is 1 mm. Moreover, the height of the overall structure is 26 mm, which is less than 40 mm of the common thermal protection structure. Pentagon channel, which combines the geometric characteristics of triangular and rectangular channel, is designed to investigate whether it can improve the thermal protection performance. Ultimately, the thermal–hydraulic and thermodynamic performance of the improved "Diamond" channel are systematically analyzed in detail as well.

The main physical properties of solid materials and cooling medium are displayed in Table 1. In the NASA X–43A program [45,46], the leading edge is made of C–C thermal insulation material. Meanwhile, a layer of SiC material is coated on its surface to prevent oxidation and Haynes–230 alloy is used for the horizontal and vertical tail. The physical properties of two high heat–resistant alloys are compared in Table 2. By balancing various factors, Inconel–625 which can further reduce the weight of hypersonic aircraft owing to its smaller density was selected as the material for active thermal protection structure.

2.2. Computational methods

Liquid water whose physical parameters are assumed not to change with temperature forasmuch as the low temperature rise is chosen as the coolant firstly. Moreover, the physical properties of Inconel–625 are supposed as constant. Throughout the research process, Reynolds number of liquid water ranges from 4000 to 22,000, resulting in the turbulence flow pattern inside the channel. Based on the assumptions, the governing equations describing the nature of flow and heat transfer in the active thermal protection channel are as follows:

Solid domain:

$$\frac{\partial}{\partial_{X_i}}\left(K_s\frac{\partial T}{\partial_{X_i}}\right)=0 \tag{1}$$

The K_S of Inconel–625 is set to 27 W/(m · K). For the three–dimensional turbulent flow in fluid domain, the Reynolds averaged Navier Stokes equations are adopted. Liquid water is considered continuous and incompressible. Furthermore, the flow and heat transfer processes are steady and the effects of gravity and radiation are ignored for testing the reliability of active thermal protection structure under the extreme condition. The viscous dissipation of the energy equation is ignored. SST k–ω model which has better effect in estimating the free shear flow combines the calculation advantages of both standard k–e model and the k –ω model by using the mixing function. Hence, SST k–ω model is selected for subsequent numerical analysis.

The governing equations are as follows:

Continuity equation:

$$\frac{\partial(\rho u_i)}{\partial_{X_i}}=0 \tag{2}$$

Momentum equation:

$$\frac{\partial}{\partial_{X_j}}\left(\rho u_i u_j\right)=-\frac{\partial\rho}{\partial_{X_j}}+\frac{\partial}{\partial_{X_j}}\left[\mu\left(\frac{\partial_{u_i}}{\partial_{X_j}}+\frac{\partial_{u_j}}{\partial_{X_i}}\right)\right] \tag{3}$$

Energy equation:

$$\frac{\partial}{\partial_{X_i}}\left(\rho u_i c_p T\right)=\frac{\partial}{\partial_{X_i}}\left(k\frac{\partial T}{\partial_{X_i}}\right)+\Phi \tag{4}$$

The governing equation of the SST k–ω model is expressed as:

$$\frac{\partial}{\partial_{X_i}}\left(\rho k u_i\right)=\frac{\partial}{\partial_{X_i}}\left(\Gamma k\frac{\partial k}{\partial_{X_i}}\right)+G_k+Y_k \tag{5}$$

$$\frac{\partial}{\partial_{X_i}}\left(\rho\omega u_i\right)=\frac{\partial}{\partial_{X_i}}\left(\Gamma\omega\frac{\partial\omega}{\partial_{X_i}}\right)+G_\omega+Y_\omega \tag{6}$$

Table 1
Main physical properties of materials.

parameter	P(kg/m3)	Cp(J/kg·K)	λ (W/m·K)	μ(kg/m·s)
Nickel base alloy	8440	430	27	\
Water	998.2	4182	0.6	0.001003

Table 2
Comparison of physical properties of two alloys.

parameter	P(kg/m3)	Cp(J/kg·K)	KS (W/m·K)	μ(kg/m·s)
Haynes–230	8970	440	11.7	\
Inconel–625	8440	430	27	\

ANSYS Fluent, which is based on the finite volume method (FVM), is applied to solve the governing equations. The convergence criterion in this study states that relative residual values are less than 10^{-3} for continuity equation and less than 10^{-6} for all other variables, or all the relative residual values are maintained basically constant. The discrete format of pressure is standard. Pressure outlet is adopted to minimize backflow and interface between solid and fluid domain is set as a no slip coupling heat transfer wall. The discrete format of momentum and energy is second–order upwind format, and solver is set to SIMPLE algorithm.

2.3. Parameter definitions

The feature size of channel section is defined as follows:

$$D_h = \frac{4S}{C} \tag{7}$$

where S and C are flow–through section area, fixed at 96 mm^2 and the perimeter of channel section, respectively.

In this paper, Reynold number (Re) is defined as:

$$Re = \frac{\rho u_m D_h}{\mu} \tag{8}$$

where u_m is average velocity at the inlet, μ and ρ are the viscosity and density of the cooling medium, respectively.

The resistance coefficient (f) of coolant is given by:

$$f = \frac{2\Delta P D_h}{\rho L (u_m)^2} \tag{9}$$

where ΔP is the pressure drop between the inlet and outlet boundary surface.

The definitions of heat transfer coefficient (h) and average Nusselt number (Nu) are expressed formulas as follows:

$$h = \frac{qA_h}{S(T_w - T_m)} \tag{10}$$

$$Nu = \frac{hD_h}{K_f} \tag{11}$$

where q and T_w are average heat flux and average temperature on fluid–solid coupling interface separately. T_m is the mean temperature of the fluid, calculated by the arithmetic mean of the inlet and outlet mass–average temperatures. K_f is thermal conductivity of coolant, and the Nu characterizing the heat convective capability of the fluid–solid coupling interface can be obtained by the formula.

The total pumping work consumed to actuate the coolant is defined as follows:

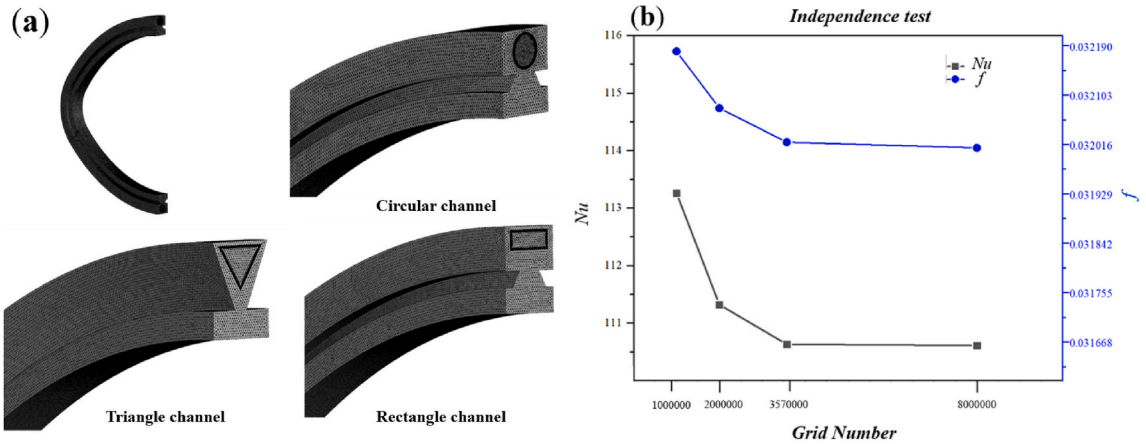

Fig. 2. Schematic diagram of grid division and results of the grid independence test (a) grid division (b) grid independence test.

$$W_P = \frac{m\Delta P}{\rho} \tag{12}$$

where m is the mass flow rate.

2.4. Grid system and independence test

Fig. 2 (a) presents schematic diagram of grid division, in which unstructured tetrahedral mesh is adopted. For sake of accurately calculating the coolant flow and heat transfer characteristics of boundary layer, 14 multi–layer dense grid near wall is applied on the contact surface between fluid and solid domain. The first layer and the global grid size are 0.8 mm and 0.02 mm, respectively. Grid growth rate is set as 1.2. Grid independence test results indicate that the deviations between grid systems with 3.57×10^6 and 8×10^6 cells are limited in ±0.5%, as depicted in Fig. 2 (b). Therefore, grid system with 3.57×10^6 cells is dense enough and applied for the following simulation.

2.5. Model validation

The Gnielinski correlation for the *Nu* and Konakof's correlation for the *f*, which are given in Eqs. (13) and (15), are applied to verify the heat transfer and flow resistance performance of the rectangular model, including straight and elbow channel, as displayed in Fig. 3.

$$Nu_0 = \frac{(f/8)(Re - 1000)Pr.M}{1 + 12.7(f/8)^{0.5}\left(Pr^{2/3} - 1\right)} \tag{13}$$

$$M = \left[1 + (D_h/L)^{2/3}\right] \tag{14}$$

Equation (13) is Gnielinski formula, which is a correlation with the highest computational accuracy so far [47,48]. *M*, as the correction coefficient whose size is related to the ratio of the feature size to overall length of the channel is given in equation (14).

$$f_0 = (1.82\lg Re - 1.64)^{-2} \tag{15}$$

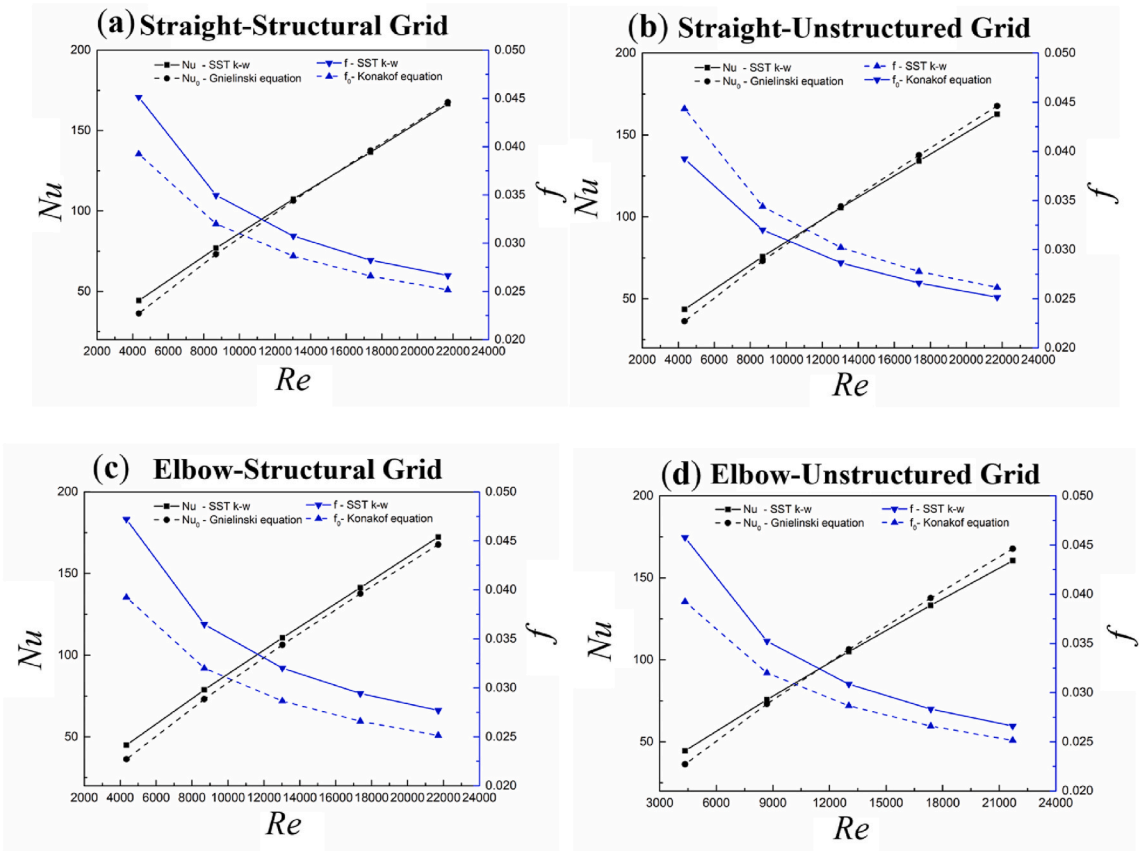

Fig. 3. Verification results of different grid types of rectangular channel.

Konakof 's formula is a common formula for calculating the *f* of channel, which is only related to *Re* [49].

It is observed in Fig. 3 that the verification results of heat transfer and flow resistance performance whose relative errors are less than 15% and 20% respectively, coincide well with the empirical formula. In addition, unstructured tetrahedral grid has higher accuracy in calculating the curved channel, thus used for following numerical simulation and analysis.

3. Results and discussion

3.1. Optimization of active thermal protection channel

For purpose of comparing the thermodynamic performance of different channels, the overall temperature distribution of circular, triangular and rectangular channel at the inlet velocity of 1.5 m/s ($Re = 13{,}000$) are analyzed, as shown in Fig. 4 (a) and (b).

Fig. 4 (a) presents the high–temperature area, in which temperature can be controlled below 500 K under the cooling of ACTPS is situated in the leading edge with the maximum heat flux. It is easier to get fluid scouring for middle of outer wall, while both sides largely rely on heat conduction of support structure, resulting in lower temperature in the middle and higher temperature on both sides. Among the three channels, outer wall temperature of triangular and rectangular channel is significantly lower than that of circular. Furthermore, outer wall temperature of rectangular channel is the lowest. It can be seen in Fig. 4 (b) that inner wall temperature is reduced not to exceed 307K. Compared with outer wall, the temperature gradient of inner wall is significantly decreased, the temperature distribution is more uniform as well. Similarly, inner wall temperature of triangular and rectangular channel is lower than that of circular channel, and the inner wall temperature of triangular channel is the lowest.

Fig. 4 (c) presents that the fluid velocity near the outer wall of the rectangular channel is even larger than that of the triangular and circular channel. Temperature decreases rapidly inside outer wall, forming a high temperature gradient, as shown in Fig. 4 (d). Otherwise, the velocity distribution results show that coolant will scour the outside in curved channel, which is subjected to high aerodynamic heating. Therefore, it is conducive to enhance the cooling performance on outer wall.

For circular channel, a conspicuous high–temperature area is formed on both sides of outer wall. The heat can only be taken away

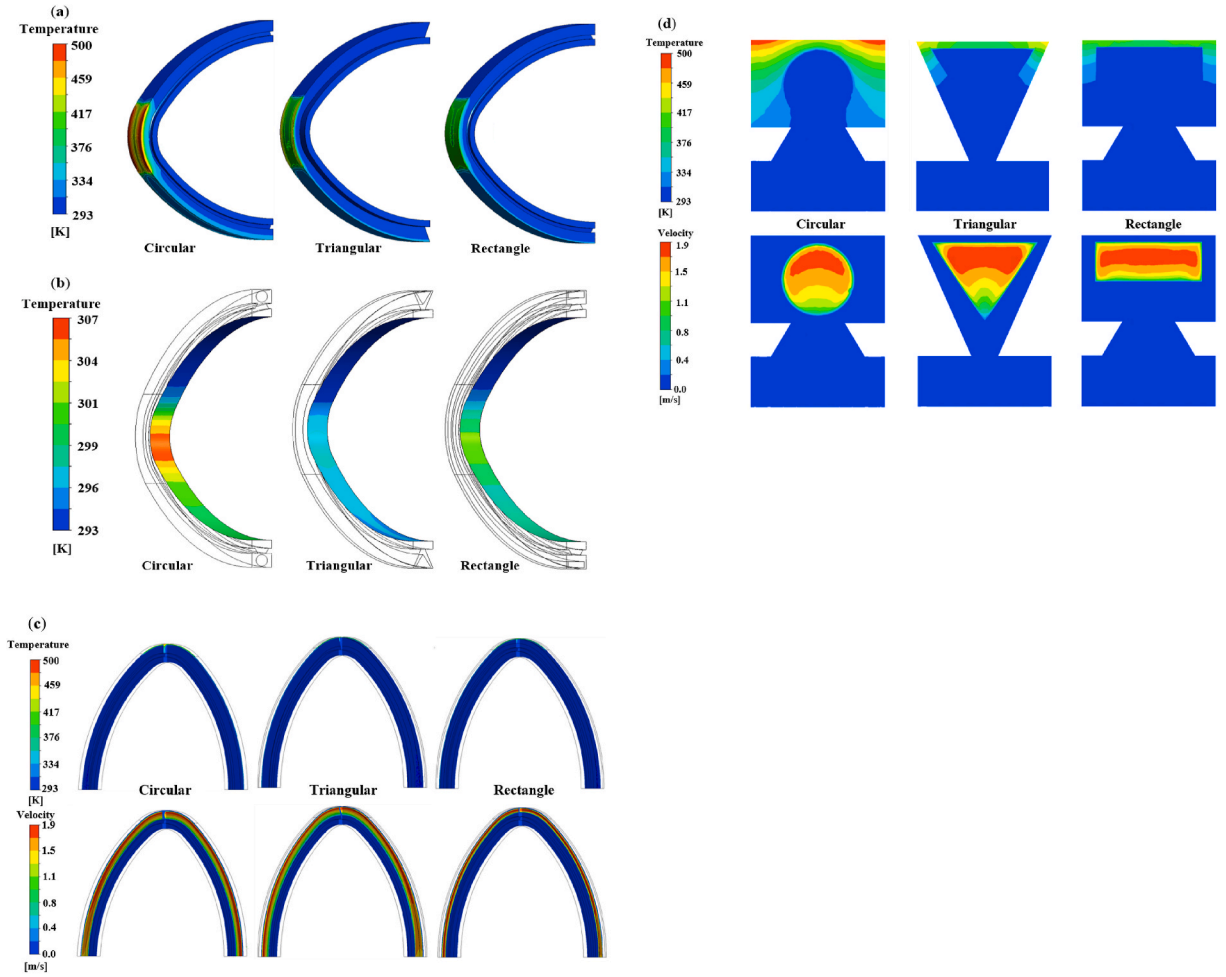

Fig. 4. Thermal-hydraulic contour of various positions in three channels (a)outer (b)inner (c) axial section (d) normal section.

by the coolant after heat transfer process of thick wall which induces a larger heat convection resistance relatively. Besides, the high–velocity scouring area of coolant in circular channel is obviously smaller than that in the triangular and rectangular channel, leading to weaker cooling performance for circular channel. For triangular channel, the heat convection performance is lower than that of the rectangular channel due to the strong wall constraints and low fluid velocity at the corners outside the channel, which result in forming a high–temperature area on both sides of the outer wall as well. For rectangular channel, the region where coolant rapidly washes the outer wall is the largest, which makes outer wall temperature lowest.

Compared with rectangular channel, triangular channel has a smaller contact area between fluid and inner wall, and the velocity is remarkably lower, leading to a smaller inward heat conduction coefficient, which can effectively prevent external aerodynamic heat from being transmitted to inner wall. Triangular and rectangular channel have their own advantages in cooling the inner and outer walls of the leading edge.

Fig. 5 present the pressure drop (ΔP) and *Nu* between different channels with velocity change, respectively. The pressure drop of coolant increases with increasing of inlet velocity, which is lower than 5500 Pa, as depicted in Fig. 5 (a). It can also be found in Fig. 5 (b) that a linear enhancement trend of *Nu* with the increase of inlet velocity. Moreover, the *Nu* of rectangular and triangular channel is significantly higher than that of circular channel, and the *Nu* of triangular channel is slightly lower than that of rectangular channel.

Subsequently, a pentagon channel which combine the geometric advantages of triangle and rectangle is designed and analyzed by numerical simulation to further strengthen the active thermal protection performance. The comparison of thermal protection performance between different channels are studied, as depicted in Fig. 6 (a)–(c). It is found in Fig. 6 (a) that pentagon channel has the best cooling performance on outer wall. When inlet velocity reaches 2.5 m/s (Re = 21,700), outer wall temperature of pentagon channel is 398.8 K, which is much lower than 433.1 K of triangular channel. However, from Fig. 6 (b), the cooling performance of pentagon channel on inner wall is not ideal. In order to ensure that the flow area of different channels are consistent, pentagon channel has a larger heat conduction area, resulting in the increase of the peak temperature of inner wall. *Nu* of the pentagon channel is higher than that of rectangular and triangular channel, which indicates the better convective heat transfer ability, as shown in Fig. 6 (c).

To improve the cooling performance limitation of the regular pentagon channel on inner wall, a new–type channel whose flow–through section shape is similar to diamond is proposed, designated as "Diamond" channel. The thermal protection performances of "Diamond" channel are shown in Fig. 6 (d)–(f). Fig. 6 (d) presents the outer wall Temperature further decreased in the *Re* range of this research. When velocity reaches 2.5 m/s (Re = 21,700), outer wall temperature of the "Diamond" model is nearly 40 K lower than that of triangle, which is only 392 K, less than 120 °C.

When the inlet velocity reaches 0.5 m/s (Re = 4300), the inner wall temperature of the "Diamond" channel is reduced by 10 K (from 335.7 K to 325.5 K) compared with that of pentagon channel, as demonstrated in Fig. 6 (e). Along with the increase of inlet velocity, inner wall temperature decreases. When the inlet velocity reaches 2.5 m/s (Re = 21,700), inner wall temperature difference between "Diamond" and triangular channel is only 1 K. In addition, Fig. 6 (f) shows that the *Nu* of "Diamond" model is higher than regular Pentagon, which reveals a better heat convection performance.

3.2. Flow and heat transfer analysis

It is necessary to explore why "Diamond" model can improve thermal protection performance significantly. Flow field characteristics of leading edge are studied of which results are presented in Fig. 7. Fig. 7 (a) shows the tangential velocity vector of three channels. It is visible that all three channels will produce symmetric longitudinal swirls. The vortex cores marked by red dotted lines are symmetrically distributed near the wall. When coolant flows in elbow, the leading edge part bends with larger curvature, thus forming special symmetric longitudinal swirls inside which are beneficial to the temperature uniformity, improving the ability of heat convection between coolant and channel wall. Compared with the acute and right angles of triangle and pentagon, we can discover from Fig. 7 (a) that "Diamond" model has relatively smooth obtuse angles whose wall constraint on coolant is reduced which leads to smoother tangential velocity vector.

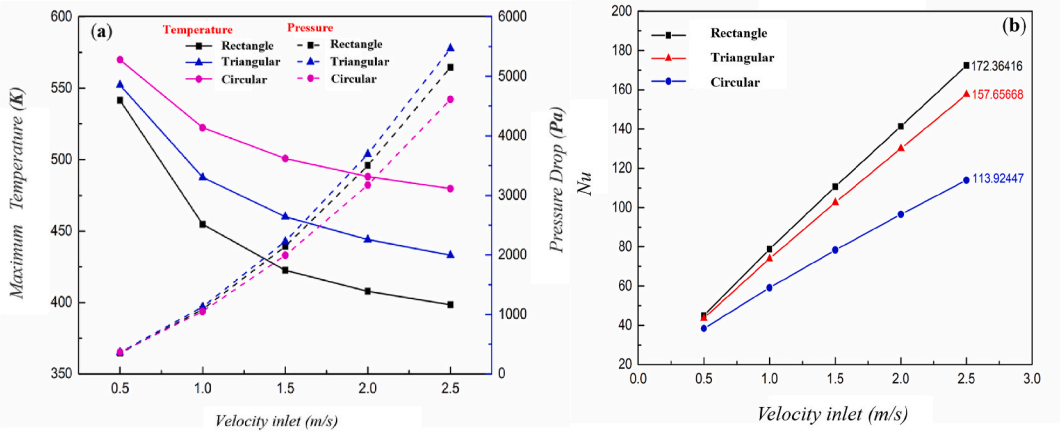

Fig. 5. Variations in thermal-hydraulic performance at different channels (a) Pressure drop (b) *Nu*.

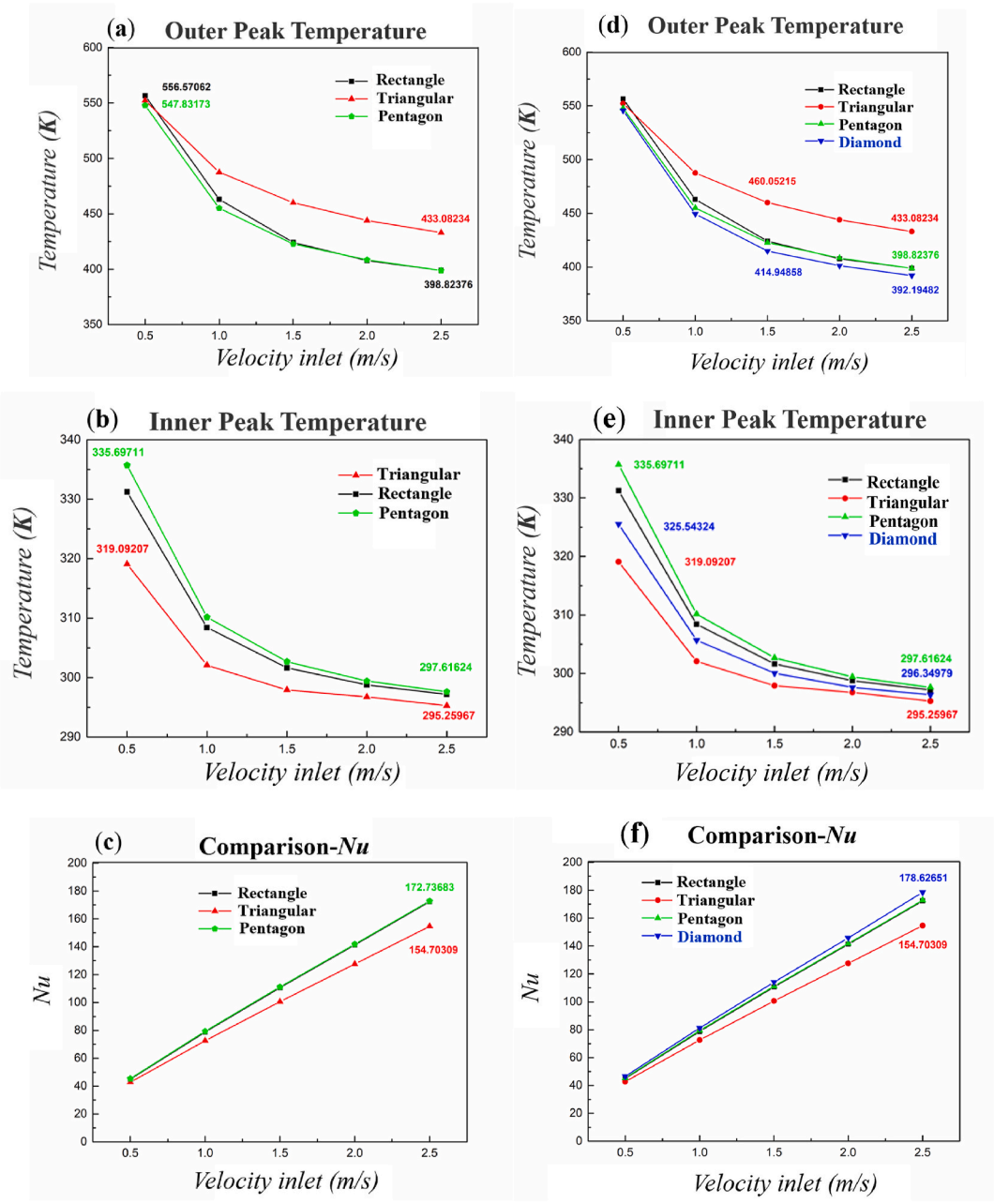

Fig. 6. Thermal protection performance of regular pentagon and "Diamond" channel (a–c) Regular pentagon (d–f) "Diamond".

Fig. 7 (b) provides the surface streamlines of the same section position as Fig. 7 (a) to better show the flow states. The streamlines are apparently constrained at the sharp corners of the triangle, while the "Diamond" model has smoother streamlines, causing a longer flow path and stronger flow mixing, which prominently improve the heat convection performance. Fig. 7 (c) reveals the influence of the symmetric longitudinal swirls on the temperature distribution in "Diamond" channel. It can be seen that the symmetric longitudinal swirls effectively promote the mixing between the hot fluid near the wall and the cold fluid inside, and produces a higher temperature gradient, which are the reasons of heat convection performance improvement. The contours of turbulence kinetic energy (TKE) and eddy viscosity in the leading edge are displayed in Fig. 7 (d) and Fig. 7 (e), respectively. The peak value of TKE concentrated near the wall, which is obviously favorable for heat convection. Eddy viscosity is the proportionality factor describing the turbulent transfer of energy as a result of moving eddies, giving rise to tangential stresses which depends on the fluid density and distance from the wall [50]. It can be obtained from Fig. 7 (e) that the largest vortex viscosity is located at the section center due to the convergence of the symmetric longitudinal swirls, which means more adequate fluid mixing. Furthermore, there are small peak region on the left and right sides singly generated by each swirl, thus making the internal cold fluid temperature more uniform. The symmetric longitudinal

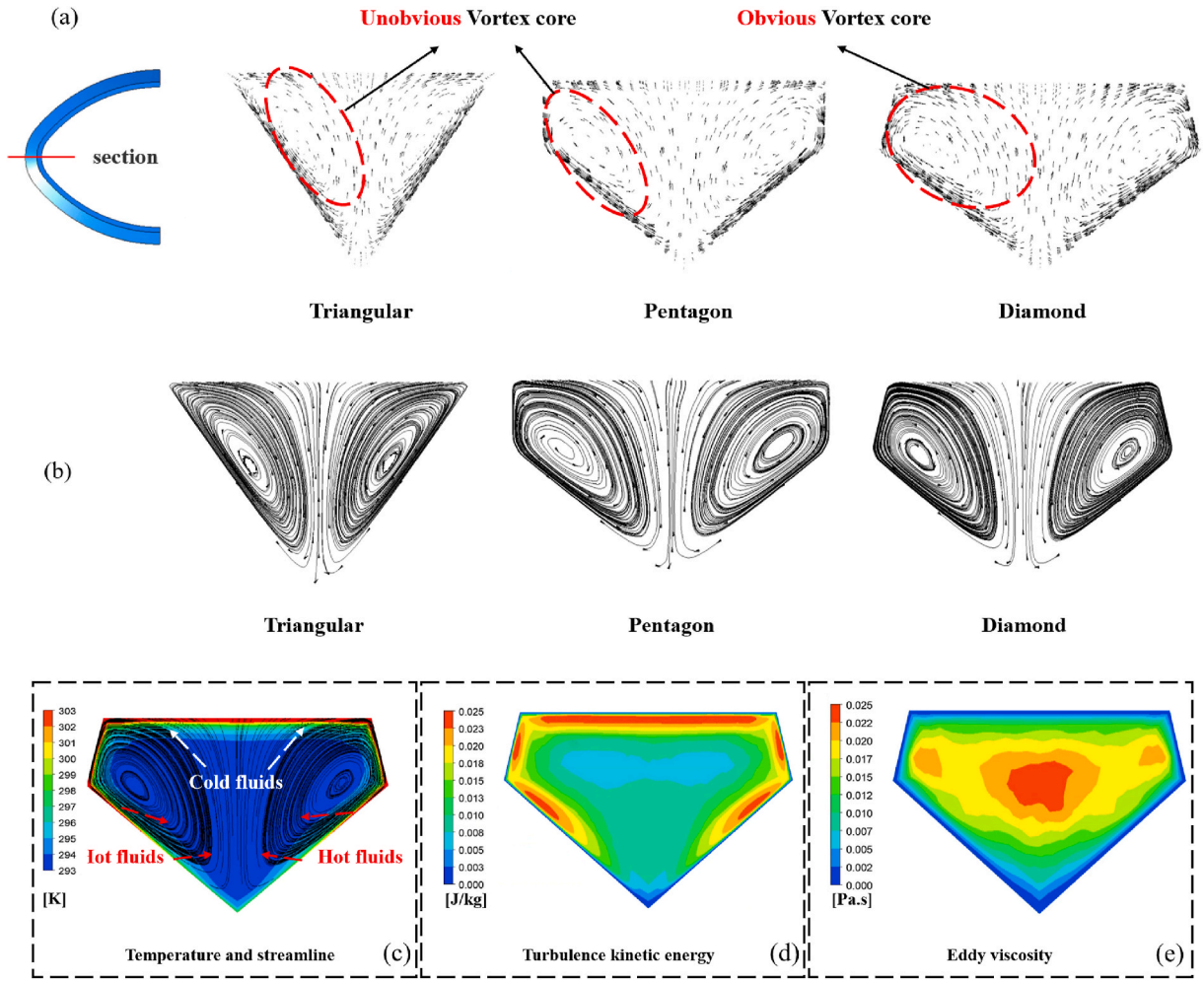

Fig. 7. Flow field characteristics of leading edge (a)Tangential velocity vector (b) Surface streamlines (c) Temperature distribution (d) TKE (e) Eddy viscosity.

swirls effectively reduce the viscous effect of the boundary layer on the internal fluid and improves the fluid mixing heat transfer effect.

3.3. Feasibility analysis of aviation kerosene

The hydrocarbon fuel is frequently used as coolant of ACTPS, which can not only realize better cooling performance, but also preheat the hydrocarbon fuel to improve the combustion efficiency. The coolant was transformed from liquid water to aviation kerosene RP–3 whose physical properties are given in Table 3. Three inlet temperatures (243 K, 253 K, 263 K) are selected to systematically analyze the thermal protection performance, as depicted in Fig. 8. When RP–3 is used as coolant, a cooling cycle is formed in the fuel tank and the ACTPS. The flight status and ambient temperature of the hypersonic aircraft will directly affect the cycle temperature and the calorific value of the fuel RP–3. Therefore, its temperature will fluctuate within a certain range. In present study, three sets of inlet temperatures (243, 253 and 263 K) are selected to verify the cooling effect of coolant RP–3 and to simulate the actual temperature of RP–3. It should be pointed out that When the aircraft speed increases, the aerodynamic heating of the ACTPS will increase, leading to the increasing of calorific value of the circulating RP–3, which will reduce the cooling effect of the coolant. Meanwhile, RP–3 flow rate must be increased to meet the requirement of active thermal protection. It should be pointed out that the negative feedback mechanism throughout the process needs to be monitored. In practice, coolant flow needs to be reasonably controlled to meet the cooling effect and fuel requirements of hypersonic aircrafts.

Table 3
Main physical properties of materials.

parameter	P(kg/m^3)	Cp(J/kg·K)	Kf (W/m·K)	μ(kg/m·s)
RP–3	800	2100	0.13	0.0001984
Water	998.2	4182	0.6	0.001003

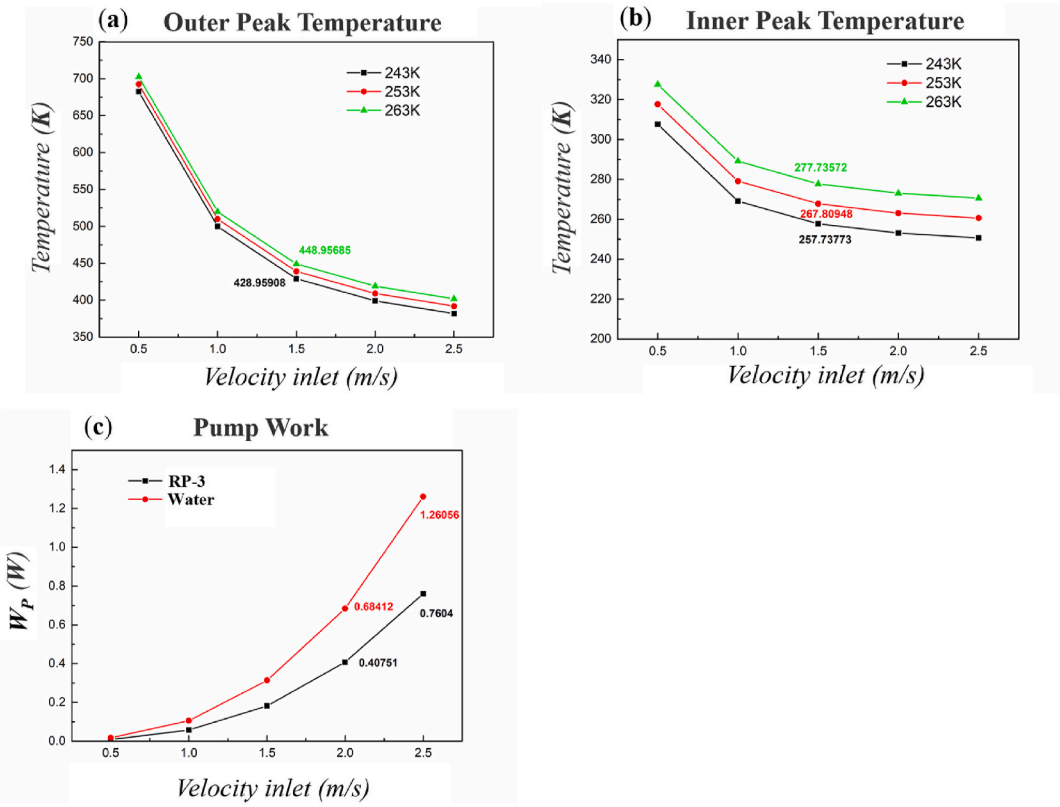

Fig. 8. Thermal protection performance with RP–3 coolant (a) outer wall (b) inner wall (c) pump power.

It can be discovered in Fig. 8 (a) that outer wall cooling performance of RP–3 is greatly affected by inlet velocity. Following with the velocity increasing from 0.5 m/s ($Re = 4300$) to 1.5 m/s ($Re = 13000$), outer wall temperature decreases from 700 K to 450 K. Due to the low freezing point of RP–3, lower inlet temperature can significantly reduce inner wall temperature. The inlet temperature of 263 K can reduce inner wall temperature to 277.7 K (only 4.5 °C) at velocity of 1.5 m/s ($Re = 13{,}000$), as presented in Fig. 8 (b). Because the dynamic viscosity of RP–3 is only 20% of liquid water, RP–3 has less flow resistance. Fig. 8 (c) present that the total pump power rises rapidly with increasing inlet velocity. Nevertheless, the pump power of RP–3 is always lower than liquid water. When inlet velocity reaches 2.5 m/s (Re = 21,700), the pump power of RP–3 is only 60% of liquid water which means a greater cooling advantage of actual application.

3.4. Optimization of "Diamond"

In order to find a better "Diamond" to meet the requirements of active thermal protection, three parameters are set, and corresponding values are given in the table, as shown in Fig. 9. L is the scouring length of outer wall, X is half of the maximum width of

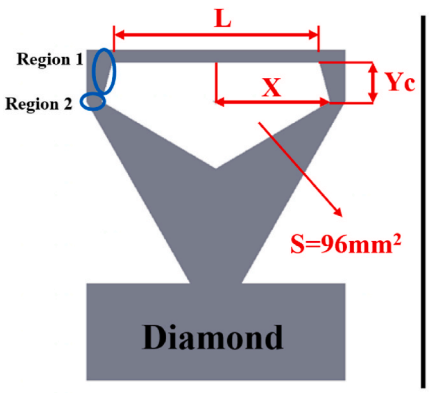

Parameter consideration

L	15.2	16.0				
Yc	0.5	1.0	1.5	2.0	2.5	3.0
X	9.6	9.2	8.8	8.4	8.0	7.6

Fig. 9. Variable parameters of "Diamond" model.

channel section, and *Yc* is the scouring height on both sides. Thermal protection performance of "Diamond" with 72 (2 × 6 × 6) situations are investigated.

The wall temperature of different parameters at the velocity of 1.5 m/s along with temperature of 253 K are demonstrated in Fig. 10 (a) and (b). It can be viewed that with the increase of *X*, the wall temperature gradually decreases. After *X* reaches 8.8 mm, it will have little influence on outer wall temperature, as shown in Fig. 10 (b). Fig. 10 (a) illustrates that *Yc* and L significantly influence the cooling performance of inner wall. Moreover, for *L* and *Yc*, 16.0 mm and 3.0 mm has the best cooling performance on both inner and outer wall, respectively. It can be obtained in Fig. 9 that when *X* increases, the area of region 1 and region 2 will be expanded and compressed, respectively. Reduction of the region 2 area reduces the heat conduction area from the outer wall to the inner wall, while it

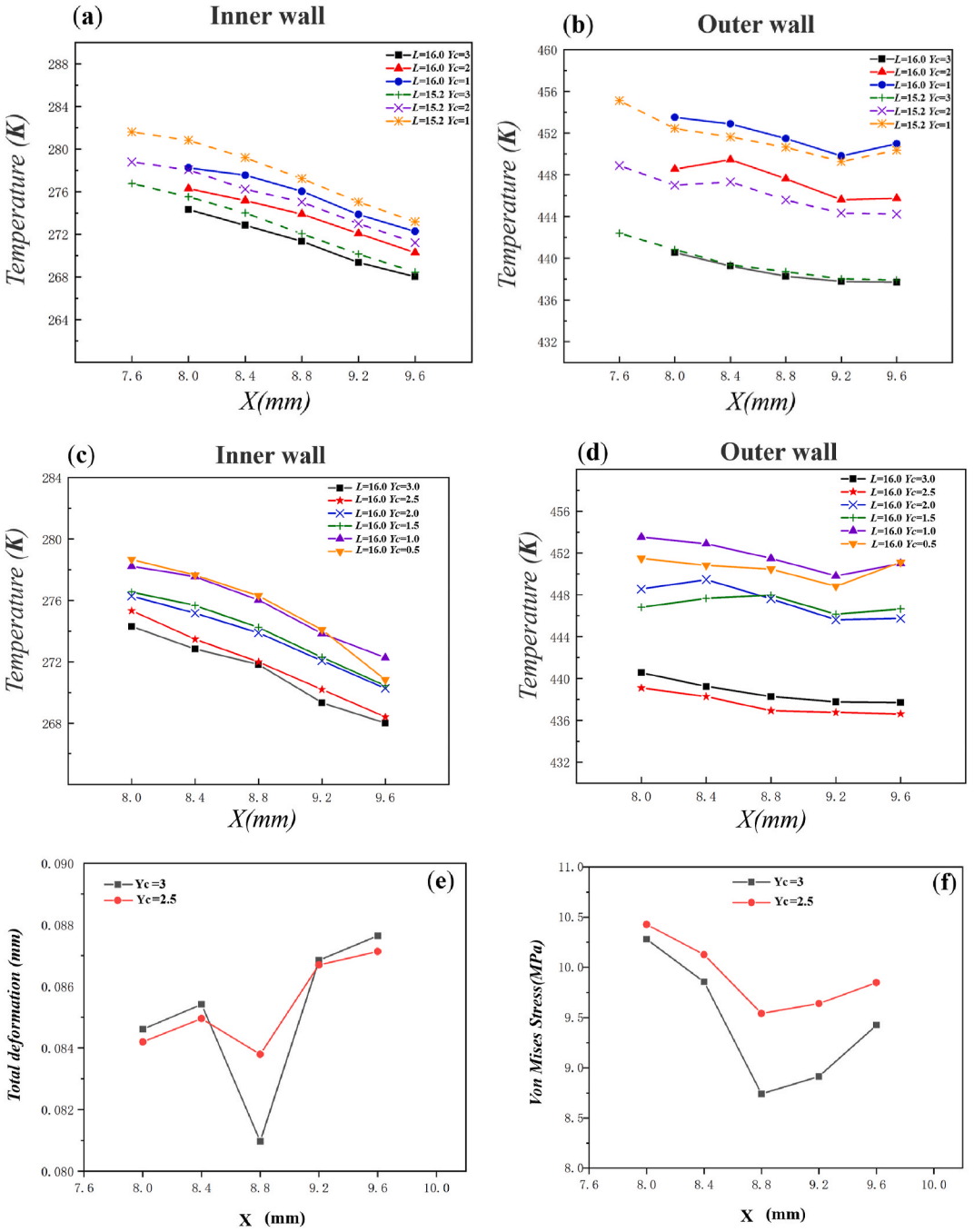

Fig. 10. Variations in temperature and thermal stress index of different "Diamond" (a)Inner wall–comparison (b) Outer wall–comparison (c) Inner wall–$L = 16$ mm (d) Outer wall–$L = 16$ mm (e) total deformation–$L = 16$ mm (f) Von mises stress–$L = 16$ mm.

will expand the scouring area of the outer wall in region 1. The cooling effect of the two on outer wall is opposite, which means coordination between both region is essential. In Fig. 10 (b), the outer wall temperature of model with $Yc = 2$, when X change from 8.0 to 8.4, At this case, the scouring area in region 1 has very little expansion, while the area compression of region 2 is the dominant influencing factor, more heat is blocked in outer wall. Therefore, the outer temperature increases slightly. Subsequently, the increasing of X significantly expands the scouring area of region 1, so the outer temperature decreases further. Similarly, in this figure, the model with $Yc = 1$, with X changing from 9.2 to 9.6, Due to the small Yc, the heat conduction area of region 2 is compressed to a small value, which blocks more heat on outer wall and causes the outer temperature to rise. Owing to the difference of Yc, the dominant influence exchange points of region 1 and region 2 on outer cooling effect are also different, so the variation range of X is different when the temperature rises.

Temperature for L = 16 mm is displayed in Fig. 10 (c) and (d). It is worth pointing out that when Yc reach 1.0 mm and 0.5 mm, Fig. 10 (c) and (d) show irregular temperature change trend, which is not allowed to present in hypersonic aircraft. It can be found from Fig. 10 (c) that with X changing from 9.2 to 9.6, the inner temperature of $Yc = 0.5$ decreases sharply, which is lower than that of $Yc = 1.0$. Similarly, with X changing from 9.2 to 9.6, the outer temperature of $Yc = 0.5$ increases sharply, which is larger than that of $Yc = 1.0$. Hence, the above two points show irregular temperature change trend for $Yc = 0.5$ and 1.0 and The smaller Yc, which has smaller scouring area in region 1, as depicted in Fig. 9, is the essence to result in sharp change in temperature, leading to the weakening of the temperature control of outer wall. It is well known that hypersonic aircrafts have high safety requirements, so $Yc = 0.5$ and 1 will bring higher security risks. The inner wall temperature is of great significance to the normal work electronic devices inside and will therefore be the primary consideration. It is found in Fig. 10 (c) that the inner wall temperature of $Yc = 3.0$ mm is slightly lower than $Yc = 2.5$ mm.

It is well known that support structure will be deformed due to non–uniform temperature distribution in practical application. For comprehensively comparing the feasibility of "Diamond", thermal stress indexes with various parameters must be analyzed. In this study, we get the following data, as depicted in Fig. 10 (e) and (f), by coupling the calculated temperature field with the structural strength in Ansys Workbench.

It can be observed in Fig. 10 (e) and (f) that von mises stress of $Yc = 3$ mm is less than $Yc = 2.5$ mm which shows a trend of decreasing firstly and then increasing with the increase of X. It is clear that $X = 8.8$ mm has the minimum value of total thermal deformation and von mises stress, which is more suitable for the ACTPS design requirements of hypersonic aircraft. When X is large, the thickness of both sides is too small, the thermal stress causes large deformation. When X is small, thermal conductivity area on both sides is too large, resulting in large temperature difference between the wall and fluid, which can also cause large deformation.

Von Mises criterion is a comprehensive concept, which takes into account the first, second and third principal stresses. It can be used to evaluate fatigue and failure. Mechanical properties test results show that the yield strength of Inconel–625 can reach 275 MPa, which is greater than the von mises stress of active thermal protection structure in this study. Meanwhile, Inconel–625 has good ductility and solder ability, which can meet the structural changes caused by small deformation.

4. Conclusions

In this study, an active thermal protection structure with several parallel channels is proposed to meet the thermal protection requirement of hypersonic aircraft. Performance of different flow–through section shapes are analyzed. Eventually, "Diamond" channel is established whose cooling performance is studied by numerical simulation comprehensively. Besides, we verify its feasibility and advantages as active thermal protection structure with RP–3 as the coolant. The main conclusions drawn in this work are as follow.

(1) The thermal protection performance of various channels in the range of Re (4300–22000) are evaluated. The peak temperature can be controlled under 575 K (302 °C) and 340 K (67 °C) on inner and outer wall, respectively. Triangular and rectangular channel have their own advantages in cooling the inner and outer walls of the leading edge. Moreover, Pentagon channel can significantly improve the cooling performance of outer wall, while inner wall cooling performance is not ideal.
(2) The cooling performance of RP–3 as a coolant is also studied in this study. Due to its low freezing point, the inlet temperature of RP–3 can be lower than liquid water, leading to a low inner wall temperature which is only 257.7 K under the inlet fluid conditions of 243 K and 1.5 m/s (Re = 53,000). Besides, outer wall temperature does not exceed 700 K, which is lower than the withstand temperature of Inconel–625, meeting the requirements of practical application. Moreover, the total pumping power of RP–3 is only 60% of liquid water.
(3) The performance of thermodynamic and mechanical properties of "Diamond" channel with various parameters are investigated under different operating conditions (Tin = 243–263K). It is found that the "Diamond" forms a more conspicuous symmetric longitudinal swirls in leading edge, which is significantly beneficial to make fluid temperature more uniform, improving the heat convection coefficient. As a result, "Diamond" with L = 16 mm, Yc = 3.0 mm and X = 8.8 mm is the most suitable for the thermal protection conditions of hypersonic aircraft whose inner wall and outer wall temperature are 271.5 K and 439.2 K, respectively. Meanwhile, the von mises stress of overall structure is much smaller than yield strength of Inconel–625, which can reach 275 MPa.

In summary, "Diamond" channel can able to provide a better thermal protection performance of hypersonic aircraft in two aspects of thermal effect and mechanical properties. Moreover, RP–3 as coolant can obtain higher efficiency than liquid water. The "Diamond" with RP–3 coolant has a good application potential in the active thermal protection for hypersonic aircraft.

Author statement

Yancong Qiao: Methodology, Data curation, Writing Original draft preparation, Investigation. **Peng Liu:** Visualization. **Wei Liu:** Methodology. **Zhichun Liu:** Conceptualization, Supervision, Founding acquisition.

Declaration of competing interest

The authors declare that they have no known competing financial interests or personal relationships that could have appeared to influence the work reported in this paper.

Data availability

Data will be made available on request.

Acknowledgment

The work was supported by the National Natural Science Foundation of China (Grant No. 52076088) and the Open Fund of State Key Laboratory of Coal Combustion (Grant No FSKLCCA2007). The authors wish to thank the reviewers for their careful, unbiased and constructive suggestions, which led to this manuscript.

Nomenclature

C_p	specific heatcapacity,J/(kg·K)
K_f	fluid mediumthermal conductivity, W/(m·K)
K_s	solid mediumthermal conductivity, W/(m·K)
FVM	finite volume method
ACTPS	active cooling thermal protection system
f	friction factor
h	heat transfer coefficient,W/(m^2·K)
k	turbulent kinetic energy(TKE),m^2/s^2
Nu	Nusselt number
Pr	Prandtl Number
P	pressure, Pa
q	heat flux per unit area,W/m^2
Re	Reynolds number
T	temperature, K
T_w	temperature of channel wall, K
T_m	averagetemperature of the fluid, K
T_{in}	inlettemperature of the fluid, K
T_{out}	outlettemperature of the fluid, K
u	fluidvelocity,m/s
ΔP	the pressure drop between the inlet and outlet, Pa/m
D_h	hydraulic diameter of different model, mm
A_b	Outer wall area, mm^2
S	Channel flow–through section area, mm^2
C	Channel circumference, mm^2
m	mass flow rate, kg/s
X	half of the maximum width of the “Diamond” model, mm
L	the scouring length of the channel, mm
Y_c	the scouring height on both sides, mm
W_p	pump work of different coolant, W

Greek symbols

α	thermal diffusivity,m^2/s
ε	turbulent dissipation rate, m^2/s^3
μ	viscosity, Pa·s
ρ	density, kg/m3
λ	materialthermal conductivity,W/(m·K)

References

[1] X.X. Chen, W.H. Liu, Z.S. Luo, et al., Research progress of aerodynamic heat of hypersonic vehicles, Aviation Weapons (6) (2014) 8–13.
[2] H. Yang, Y. Ji, J. Lin, et al., Investigation into the Influences of Turbulence Models on Heating Prediction of Hypersonic Inflatable Aerodynamic Decelerator, 2022.
[3] H.Z. Qiu, H. Jiang, Foreign cruise missile materials and technology, Aerospace Mater. Technol. 28 (4) (1998) 9–14.
[4] Yang YZ,Yang JL, Fang DN. Research Progress on Thermal Protection Materials and Structures of Hypersonic Vehicles[J].
[5] Craig Covault, Air Force X–37B wings into space, Aero. Am. (2010).
[6] W.S. He, Overview of scramjet development, J. Rocket Propul. 31 (1) (2005) 29–32.
[7] Y.S. Guo, W. Jiang, A new calorimeter for measuring heat sink of endothermic hydrocarbon fuels, Chin. J. Chem. 60 (1) (2002) 55–59.
[8] J. Qin, S.L. Zhang, W. Bao, et al., Effect of recooling cycle on performance of hydrogen fueled scramjet, Int. J. Hydrogen Energy 37 (23) (2012) 18528–18536.
[9] J. Ren, Y. Tan, Thermal protection techniques of ramjet combustor, J. Rocket Propul. (2006).
[10] W. Luo, H. Han, R. Jiang, et al., 3D numerical investigation of trans-critical heat transfer enhancement in regeneration cooling channel with crescent rib[J], Int. J. Therm. Sci. 172 (2022), 107287.
[11] Y.D. Wu, et al., Advanced thermal protection method and its application prospect in aircraft, 1, Aerospace Gen. Technol. 1 (1) (2017) 72–77.
[12] N. Gascoin, G.A. Abraham, P. Gillard, Thermal and Hydraulic Effects of Coke Deposit in Hydrocarbon Pyrolysis process[C], Aiaa International Space Planes & Hypersonic Systems & Technologies Conference, 2012.
[13] L. Taddeo, N. Gascoin, I. Fedioun, et al., Dimensioning of automated regenerative cooling: setting of high–end experiment, Aero. Sci. Technol. 43 (2015) 350–359.
[14] L. Qin, G. Zhao, Q. Yang, et al., [Design of an implantable sensor for detecting uterine musculature deformation and analysis of its performance], J. Biomed. Eng. 27 (2) (2010) 292–296.
[15] Z. Cong, J. Qin, Q. Yang, et al., Indirect measurement method of inner wall temperature of scramjet with a state observer, Acta Astronaut. 115 (2015) 330–337.
[16] P.A. Jian, A. Tz, A. Wlz, et al., Overall thermal performances of backward film cooling with simulated surface thermal barrier coatings at various walls, Case Stud. Therm. Eng. (2022) 32.
[17] B. Cai, J.W. Li, A.M. Tian, Design of Liquid Rocket Engine [M], Beihang University Press [et al], 2011.
[18] A. Mk, H. Dong, A. Bjl, et al., Flow characterization of microscale effusion and transpiration air cooling on single blade, Case Stud. Therm. Eng. (2022) 31.
[19] D.E. Glass, Ceramic Matrix Composite (CMC) Thermal Protection Systems (TPS) and Hot Structures for Hypersonic Vehicles[C], 15th AIAA International Space Planes and Hypersonic Systems and Technologies Conference, 2008.
[20] S.S. Jin, Study on Transpiration Cooling of Thrust Chamber and Blunt Nose Cone of Liquid Rocket Engine [D], Tsinghua University, 2008.
[21] Q.Y. Zhang, Structure and Cooling Design of Thrust Chamber of Liquid Rocket Engine [D], Tsinghua University, 2012.
[22] W. Zinner, D. Haeseler, C. Maeding, et al., Development of Advanced Technologies for Future Cryogenic Thrust Chamber applications[C]//Joint Propulsion Conference & Exhibit, 2013.
[23] D.E. Glass, A.D. Dilley, H.N. Kelly, Numerical analysis of convection/transpiration cooling, J. Spacecraft Rockets 38 (1) (2001) 15–20.
[24] B. Robbers, B. Anderson, W. Hayes, et al., Platelet Devices – Limited Only by One's Imagination[C], Aiaa/asme/sae/asee Joint Propulsion Conference & Exhibit, 2013.
[25] D. Haeseler, C. Maeding, V. Rubinskiy, et al., Experimental Investigation of Transpiration Cooled Hydrogen–Oxygen Subscale chambers[C], Aiaa/asme/sae/asee Joint Propulsion Conference & Exhibit, 2013.
[26] H. Otsu, K. Fujita, T. Ito, Application of the Transpiration Cooling Method for Reentry Vehicles[C]/, Aiaa Aerospace Sciences Meeting & Exhibit, 2007.
[27] H. Su, J. Wang, F. He, et al., Numerical investigation on transpiration cooling with coolant phase change under hypersonic conditions, Int. J. Heat Mass Tran. 129 (FEB) (2019) 480–490.
[28] Ronald S. Fry, A century of ramjet propulsion technology evolution, J. Propul. Power 20 (1) (2004) 27–58.
[29] R. Bo, Numerical model development and validation for hydrocarbon fuel supercritical heat transfer with endothermic pyrolysis[J], Acta Aeronautica Astronautica Sinica 32 (12) (2011) 2220–2226.
[30] S. Liu, B. Zhang, Effects of active cooling on the metal thermal protection systems[J], Aero. Sci. Technol. 15 (7) (2011) 526–533.
[31] Y. Hua, Y. Wang, H. Meng, Numerical study on turbulent convective heat transfer with n–heptane under supercritical pressures[J], Acta Aeronautica Astronautica Sinica 132 (42) (2010) 15046–15059.
[32] Z. Chen, L. Wang, Study of heat transfer of cryogenic methane under supercritical pressure with consideration of thermal conduction in engine cooling channel walls, Hangkong Xuebao/Acta Aeronautica et Astronautica Sinica 34 (1) (2013) 8–18.
[33] H. Fang, T. Yu, Y. Li, Research on endothermic hydrocarbon fuels, Missiles and Space Vehicles (2005).
[34] Sylvia MJ, Matthew JG, Dan L. Development of New TPS at NASA Ames Research Center,AIAA–2008–2560[R].Reston.
[35] K.D. Song, H.C. Sang, S.J. Scotti, Transpiration cooling experiment for scramjet engine combustion chamber by high heat fluxes, J. Propul. Power 22 (1) (2006) 96–102.
[36] K. Kan, R. Bowersox, R. Srinivasan, et al., Experimental and numerical studies of diamond–shaped injector in a supersonic flow, J. Propul. Power 26 (2) (2010) 373–376.
[37] N. Vermaak, L. Valdevit, A.G. Evans, Materials property profiles for actively cooled panels: an illustration for scramjet applications, Metall. Mater. Trans. 40 (4) (2009) 877–890.
[38] A.V. Attetkov, P.A. Vlasov, I.K. Volkov, Steady-State Temperature Field in a Separator System Featuring Active Thermal Protection with Anisotropic Properties, 2020.
[39] Q.S. Ma, H.T. Liu, Y. Pan, et al., Research progress of application of C/SiC composites in scramjet, J. Inorg. Mater. 28 (3) (2013) 247–255.
[40] Y.P. Hou, C. Hou, X.P. Wan, et al., Analysis of influencing parameters of convective active cooling structure, Solid Rocket Technol. 39 (1) (2016) 90–94.
[41] H.A. Jie, B. Wxya, Active flow control by a novel combinational active thermal protection for hypersonic vehicles, Acta Astronaut. 170 (2020) 320–330.
[42] S. Liu, B. Zhang, Study on active cooling efficiency of active cooling metal thermal protection system with transpiration, Acta Astronautica Sinica 32 (2) (2011) 433–438.
[43] M. Chen, Y. Hu, Z. Han, et al., Study on influence of forced vibration of cooling channel on flow and heat transfer of hydrocarbon fuel at supercritical pressure, Therm. Sci. (2021).
[44] L.N. Peng, G.Q. He, P.J. Gui, et al., Experimental and numerical study on active cooling of high temperature resistant composites, Acta Astronautica Sinica 29 (5) (2008) 1668–1672.
[45] Y.L. Chen, The requirement of materials for hypersonic aircraft, Aviation Maintenanc Eng. (2) (2004) 20–22.
[46] H.K. Rivers, D.E. Glass, Advances in hot–structure development, in: K. Fletcher (Ed.), Thermal Protection Systems and Hot Structures, 2006.
[47] V. Gnielinski, New equations for heat and mass transfer in turbulent pipe and channel flows [J], Int. Chem. Eng. (1976).
[48] V. Gnielinski, On heat transfer in tubes, aug, Int. J. Heat Mass Tran. 63 (2013) 134–140.
[49] H. Xiao, Z.M. Dong, Z.C. Liu, et al., Heat transfer performance and flow characteristics of solar air heaters with inclined trapezoidal vortex generators, Appl. Therm. Eng. (2020), 115484.
[50] P. Jarvis, B. Jefferson, J. Gregory, et al., A review of floc strength and breakage, Water Res. 39 (14) (2005) 3121–3137.